Progress in MHSP Electron Multiplier Operation

J. M. Maia, D. Mörmann, A. Breskin, R. Chechik, J. F. C. A. Veloso, and J. M. F. dos Santos

***Abstract*—The microhole and strip plate (MHSP) gas electron multiplier was studied as a stand-alone device or in combination with a cascade of gas electron multipliers (GEMs), for X-ray and UV-photon detection. An MHSP operating in Ar/5%Xe yielded gains above 10^4 and energy resolutions of about 14% FWHM for 5.9-keV X-rays. Gains as high as 10^7 were reached in a 3-GEM/MHSP gaseous photomultiplier operating in an $Ar/5\%CH_4$; the ion back-flow ratio to the top of the first GEM could be reduced to $\sim$2%. Two-dimensional (2-D) imaging was performed using signals induced by avalanche ions on a wedge and strip (W&S) readout cathode, placed at close proximity to the anode strips; position resolution of 200–250 μm FWHM for 5.9-keV X-rays was measured.**

***Index Terms*—Gas electron multiplier (GEM), gaseous photomultipliers, ion back-flow ratio, microhole and strip plate (MHSP), two-dimensional (2-D) imaging.**

I. Introduction

SINCE its introduction, the gas electron multiplier (GEM) [1] has been widely studied and used in many different applications, as a single multiplying element or in multipliers cascading several GEMs [2]. The recently introduced microhole and strip plate (MHSP) [3] combines a GEM and a microstrip (MS) amplification structures in a single element. Like the GEM, the MHSP can be produced with advanced flexible printed circuit board (PCB) technology; its performance as a stand-alone multiplier [4] and in cascaded multi-GEM/MHSP elements [5], [6] has been extensively investigated. It has been recently demonstrated that the use of a MHSP as a last multiplication element in a GEM's cascade, dramatically reduces the fraction of back-flowing avalanche ions [6], compared to a multi-GEM [7] device. This is of a prime importance in many applications, reducing the probability of ion-induced secondary effects. In this work we present and discuss the recent progress with the MHSP multiplier: gains in $Ar/5\%CH_4$ and Ar/5%Xe gas mixtures, avalanche-ion back-flow reduction and two-dimensional (2-D) imaging. The performance obtained in X-ray and single-photon detection is presented.

Manuscript received November 12, 2003. This work was supported in part by the Fundação para a Ciĕncia e a Tecnologia (FCT), Lisbon, Portugal, through project POCTI/FNU/49553/02 of the Instrumentation Centre (unit 217/94), Physics Department, University of Coimbra, by the Israel Science Foundation, and by the Planning and Budgeting Committee of the Council for Higher Education in Israel.

J. M. Maia was with the Weizmann Institute of Science, 76100 Rehovot, Israel, on leave from the University of Coimbra, 3004-516 Coimbra, Portugal, and the University of Beira-Interior, 6201-001 Covilhã, Portugal. He is now with the University of Coimbra, 3004-516 Coimbra, Portugal, and also with the University of Beira-Interior, 6201-001 Covilhã, Portugal (e-mail: jmaia@gian.fis.uc.pt).

D. Mörmann, A. Breskin and R. Chechik are with the Weizmann Institute of Science, 76100 Rehovot, Israel.

J. F. C. A. Veloso is with the University of Coimbra, 3004-516 Coimbra, Portugal, and also with the University of Aveiro, 3810-193 Aveiro, Portugal.

J. M. F. Dos Santos is with the University of Coimbra, 3004-516 Coimbra, Portugal.

Digital Object Identifier 10.1109/TNS.2004.832606

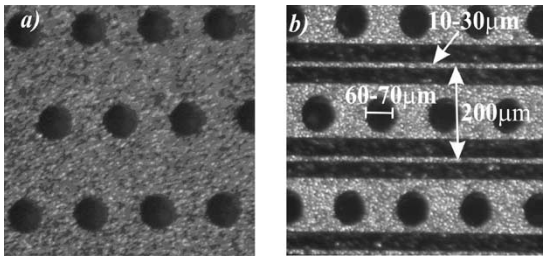

Fig. 1. Photomicrographs of the MHSP electron multiplier: (a) top side and (b) bottom side.

II. Operation Principles

The MHSP consists of two independent charge-amplification stages; they are micro patterned on a single thin insulating plate, metalized on both faces, Fig. 1. The top side shows a GEM-like pattern of holes [Fig. 1(a)]; the bottom side has a standard MS pattern [8], with the holes centered on the wide cathode strips while the anode strips run between them.

Present MHSPs are produced using 50 μm thick Kapton foil with 5 μm copper clad coating on both sides; the active area is $2.8 \times 2.8\ \mathrm{cm}^2$. Typically, the bi-conical holes have 40 to 50 μm diameter in the Kapton and 60 to 70 μm diameter in the copper layer, with a density of about 40 $\mathrm{holes/mm}^2$. The optical transparency is $\cong$7%. The microstrip pattern [Fig. 1(b)[has 200 μm pitch with anode and cathode widths of 10 to 30 μm and 100 to 120 μm, respectively.

A schematic diagram of the MHSP operating principle is depicted in Fig. 2. Voltage differences are established between the top surface and the cathode strips, as well as between the cathode and anode strips, which result in high electric fields in the holes and around the anode strips. The electric fields above and below the MHSP control the charge transport into the holes and toward the anode strips, and are defined by additional electrode planes.

Electrons produced by radiation in the gas volume above the MHSP, photoproduced at a photocathode, or transmitted from preceding amplifying elements, are focused into the holes, where a strong dipole electric field generates an avalanche. The avalanche electrons are extracted toward the anode strips where they are further multiplied in the strong electric field and collected.

It is important to note that most of the avalanche ions produced at the anode strips are collected on the nearby electrodes: the cathode strips and the cathode plane placed below the MHSP. A small fraction of the avalanche ions flows back to the MHSP top electrode and to the elements preceding the MHSP

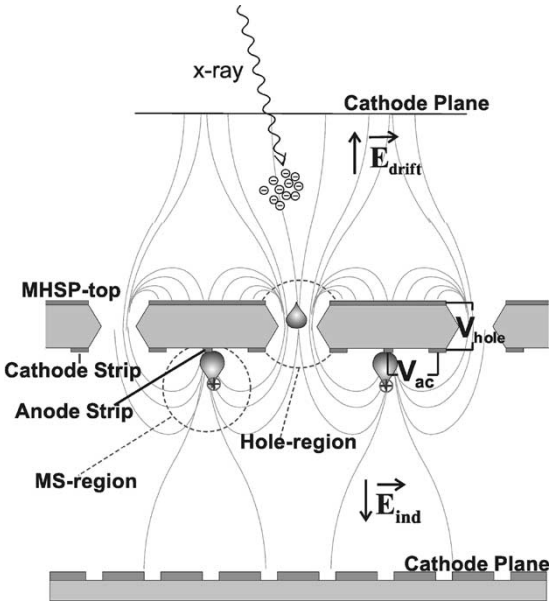

Fig. 2. Schematic diagram of the MHSP and its operating principle. Charges deposited above the MHSP by radiation, e.g., an X-ray photon, are focused into a hole and multiplied; avalanche electrons are transported toward the anode strips and multiplied in a second avalanche process. A part of the avalanche ions are collected at the cathode plane localized below the MHSP.

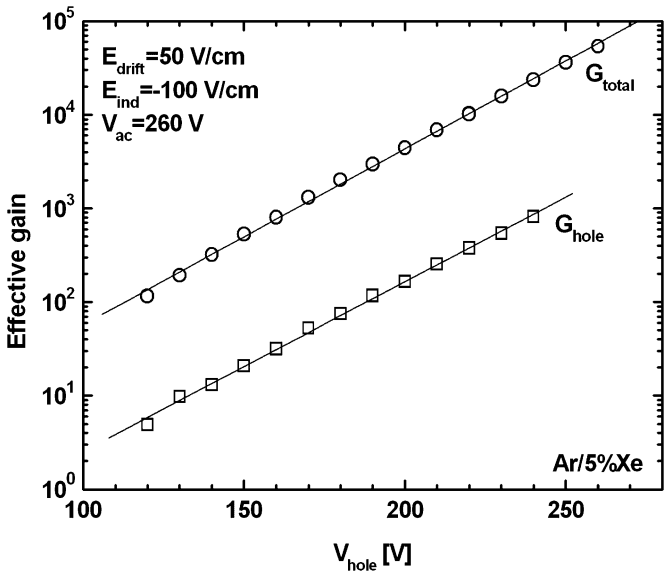

Fig. 3. Total and hole effective gains of a single MHSP operated in Ar/5%Xe mixture at 1 atm, as function of the voltage difference across the hole $\mathrm{V_{hole}}$ measured with anode strips pulses induced by 5.9-keV X-rays. The error bars are within the symbols. The MHSP was mounted between two meshes at a distance of 3.0 mm. The electronic chain was calibrated for absolute gain determination, using a calibrated capacitor directly connected to the charge pre-amplifier input and to a precision pulse generator.

[6]. This is of a net advantage compared to the situation in GEMs, where all ions from the final avalanche flow back to the GEM top electrode and to previous GEMs in the cascade [7]. In the MHSP, the *ion back-flow ratio*, namely the ratio of the number of ions collected on the MHSP top and on preceding electrodes to the number of electrons collected at the anode strips, is substantially reduced. Moreover, the anode strips avalanche is totally screened by the MHSP's substrate, allowing almost full suppression of avalanche-induced photon feedback, highly desired when the multiplier is coupled to a photocathode of a gaseous photomultiplier [9].

The small distances between the anode and cathode strips, of less than 50 μm, result in a fast collection of the avalanche ions, and signals with rise times of $\sim$10 to 30 ns are measured on the anode strips [5]. Event localization can be practiced by measuring the ion-induced charge on a patterned cathode as discussed in Section III-D, or the induced charge on the anode strips and on a structured MHSP top electrode [3].

III. Operational Characteristics

A. Gain

Fig. 3 presents the total and the hole effective gains (namely, the product of the real gain and the efficiency to focus the electrons into the holes) for a single MHSP operated in an Ar/5%Xe mixture as function of the voltage difference across the hole, $\mathrm{V_{hole}}$, maintaining the anode-to-cathode voltage, $\mathrm{V_{ac}}$, at 260 V. The MHSP anode-strip width was 30 μm, while the hole diameter was 40/60 μm in the Kapton/copper. The electric fields in the absorption/drift and in the induction regions were kept constant at 50 and ~ -100 V/cm, respectively. For the above conditions, total gain up to 5×10^4 was obtained. The total gain variation with $\mathrm{V_{hole}}$ shows the characteristic exponential behavior of proportional charge avalanche processes. The same behavior is seen for the gain variation with $\mathrm{V_{ac}}$.

The hole effective gain was determined from the ratio of the total effective gain obtained for X-ray interactions occurring in the drift region and of the gain of the interactions occurring in the induction region [4]. While the first type of events undergoes charge multiplication in both holes and anode strips, the second ones undergo charge multiplication only in the anode strips. As shown in Fig. 3, hole effective gains of the order of 10^3 were obtained, similar to that of a single GEM.

Fig. 4 presents a cascade of 3-GEMs followed by a MHSP, with a CsI photocathode evaporated on the top of the first GEM. The total effective gain obtained with this photodetector, with $\mathrm{Ar/5\%CH_4}$ gas mixture, as function of $\mathrm{V_{ac}}$ is presented in Fig. 5 for different $\mathrm{V_{hole}}$ values. The MHSP anode-strips width was 10 μm and the hole diameter was 50/70 μm in the Kapton/copper. The operation conditions were optimized for efficient photoelectron extraction from the photocathode and transmission through the first GEM, namely maintaining a high electric field at the photocathode surface by operating GEM1 at gain > 100, and keeping the drift electric field at 0 by inter-connecting the photocathode and the mesh.

Total effective gains exceeding 10^7 were obtained [6], about an order of magnitude higher than those obtained with a similar 4-GEMs cascade photodetector [7]. The high gain ensures very good single-photon detection capability when employing such multiplying structures within gaseous photomultipliers [9].

B. Response to X-Rays and Single-Photon Detection

Fig. 6 depicts a typical pulse-height distribution obtained with a MHSP gas detector for 5.9-keV X-rays, in the conditions described for Fig. 3, with $\mathrm{V_{hole}} = 250$ V and $\mathrm{V_{ac}} = 210$ V. The total effective gain was $\sim 5 \times 10^3$. The MHSP anode-strip

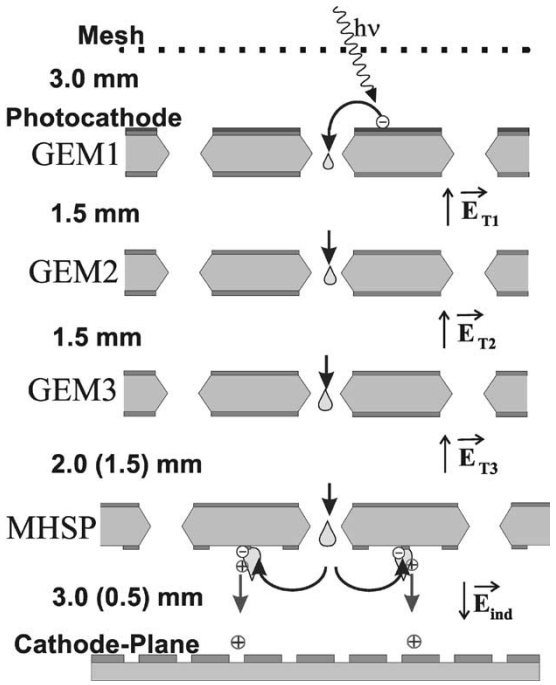

Fig. 4. Schematic view of a 3-GEMs/MHSP gaseous photomultiplier. A CsI reflective photocathode is evaporated on the top electrode of the first GEM. Photoelectrons are released to the gas by UV-photons, and are extracted and focused to the GEM1 holes.

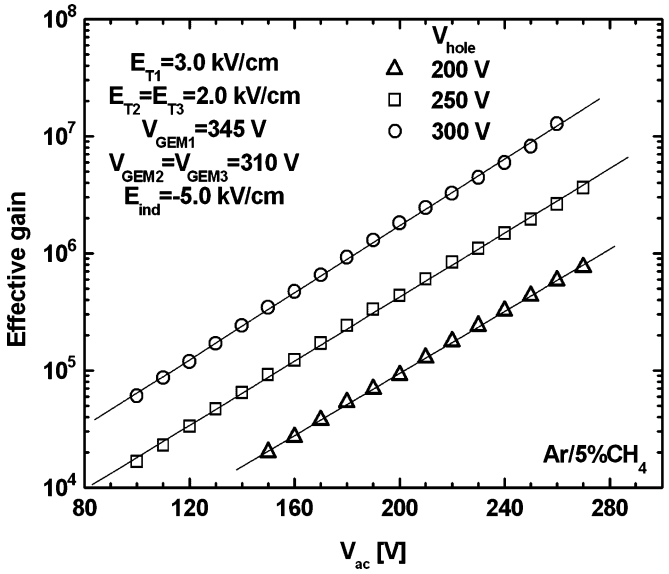

Fig. 5. Total effective gain, obtained by current measurement, of a cascaded 3-GEMs/MHSP gaseous photomultiplier operated in $\mathrm{Ar}/5\%\mathrm{CH_4}$ gas mixture at 1 atm, as function of anode-to-cathode strips voltage $\mathrm{V_{ac}}$ for several $\mathrm{V_{hole}}$ values. The effective gain of the photodetector is determined by the electron current collected on the anode strips, normalized to the photoelectron current of the electrons emitted from the photocathode. The error bars are within the symbols.

width was 30 μm, while the hole diameter was 40/60 μm in the Kapton/copper. The salient spectral features include the full energy absorption peak from X-ray interactions in the absorption region and the Ar K fluorescence escape peak. Given the small gain at the anode strips ($\leq$ 30), events resulting from X-ray interactions in the induction region, below the MHSP, appear within the noise at the low end of the spectrum. An energy resolution of 14% (FWHM) was obtained for the described conditions.

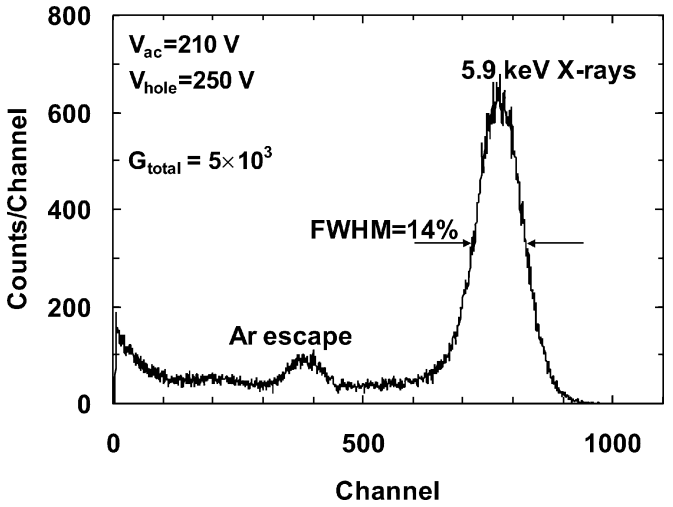

Fig. 6. Pulse-height distribution for 5.9-keV X-rays, obtained with a single MHSP operating in Ar/5%Xe mixture at 1 atm, for $\mathrm{V_{hole}} = 250\ \mathrm{V}$, $\mathrm{V_{ac}} = 210\ \mathrm{V}$, $\mathrm{E_{drift.}} = 50\ \mathrm{V/cm}$ and $\mathrm{E_{ind}} = -100\ \mathrm{V/cm}$. The pulse signals were recorded from the anode strips. The data corresponds to an irradiated MHSP surface of 20 mm in diameter. The MHSP was mounted between two meshes at a distance of 3.0 mm.

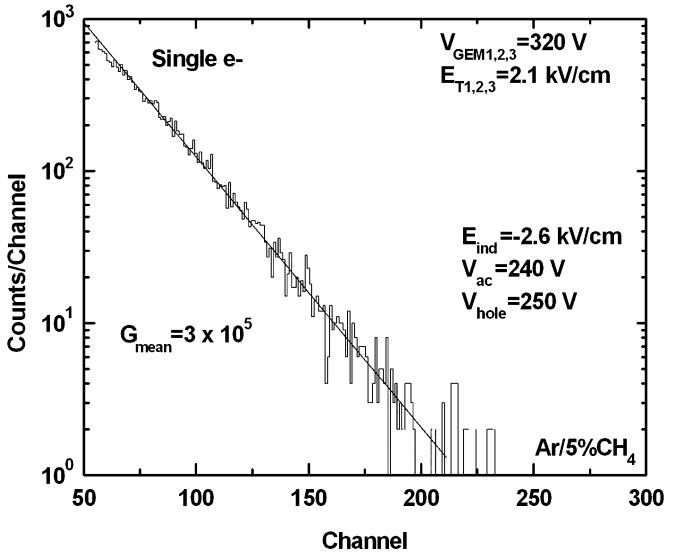

Fig. 7. Pulse-height distribution for single UV-photons obtained in a 3-GEMs/MHSP gaseous photomultiplier operated in $\mathrm{Ar}/5\%\mathrm{CH_4}$ gas mixture at 1 atm. The ion-induced signals were recorded from the cathode plane below the MHSP. An exponential fit to the data yields an apparent average gain of 3×10^5; the distribution shows no secondary effects.

Fig. 7 depicts a typical exponential pulse-height distribution obtained with the 3-GEMs/MHSP gaseous photomultiplier (see Fig. 4) for single UV-photons. In this case, the pulse signals were recorded from the positive ions collected at a cathode plane placed 0.5 mm below the MHSP. An exponential fit to the data yields an average apparent gain of 3×10^5. Since the charge signal amplitude at the cathode plane is $\sim$40% of the anode-strips signal, the anode strips have an average apparent gain of 8×10^5. Neither saturation effects, nor secondary ones were noticed at these high gains, as reflected from the purely exponential behavior of the distribution.

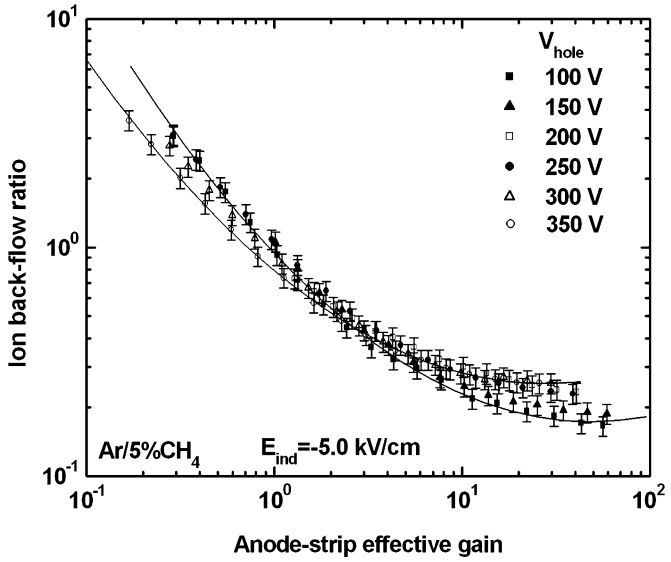

Fig. 8. Ratio between the number of ions propagating backward through the holes and the number of electrons collected at the anode strips of a MHSP, in $\mathrm{Ar}/5\%\mathrm{CH_4}$ gas mixture at 1 atm, as function of the anode-strip effective gain (by varying $\mathrm{V_{ac}}$), for several $\mathrm{V_{hole}}$ values.

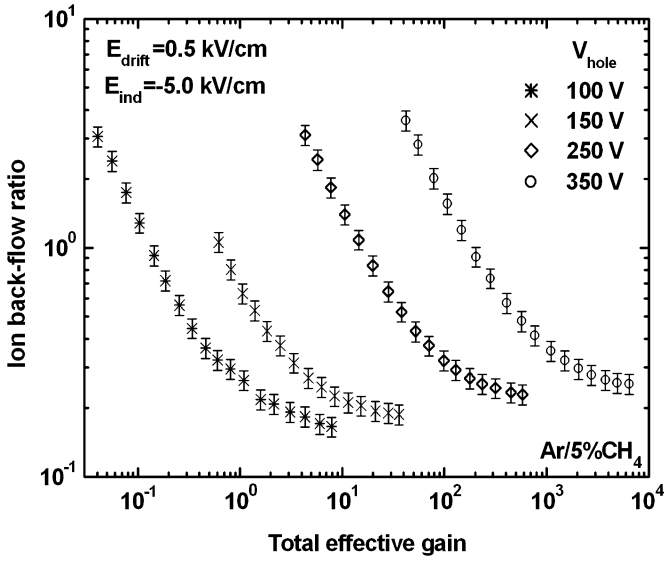

Fig. 9. Ratio between the number of ions propagating backward through the holes and the number of electrons collected at the anode strips of a MHSP, in $\mathrm{Ar}/5\%\mathrm{CH_4}$ gas mixture at 1 atm, as function of the MHSP total effective gain (by varying $\mathrm{V_{ac}}$), for several $\mathrm{V_{hole}}$ values.

C. Ion Back-Flow

The ion back-flow in MHSPs and in a cascaded 3-GEMs/MHSP gaseous photomultiplier was studied by measurement of currents (current mode) [6], using a MHSP with anode-strip width of 10 $\mu\mathrm{m}$ and the hole diameter of 50/70 $\mu\mathrm{m}$ in the Kapton/copper. Since the final avalanche occurs at the anode strips, the avalanche ions can be collected at the cathode strips and at the cathode plane placed below the MHSP (Figs. 2 and 4). Only a small fraction of the ions produced at the anode strips, together with those produced in the hole, will backflow toward the MHSP upper-region. The ion back-flow ratio, defined in Section II above, was measured for a single MHSP placed 4 mm below a semi-transparent CsI-photocathode, and 3 mm above the cathode plane; it was derived from the ratio between the sum of ion currents on the MHSP top electrode and on the photocathode, and the electron current on the anode strips. The photocathode was illuminated with UV-photons.

In Fig. 8 we present the ratio between the number of ions propagating backward through the holes and the number of electrons collected at the anode strips, as function of the anode strip gain (by varying $\mathrm{V_{ac}}$), for different $\mathrm{V_{hole}}$ values. Some of the ions are collected on the MHSP top electrode, while the rest drift toward the preceding element; their fraction depends on the ratio between the electric field in the region above the MHSP to the field in the holes (defined by $\mathrm{V_{hole}}$). As shown, the ion back-flow ratio decreases with increasing $\mathrm{V_{ac}}$, and is nearly independent of $\mathrm{V_{hole}}$. Values in the range of 17%–25% can be obtained for the ion back-flow ratio. This compares favorably with the 100% ion back-flow ratio in GEMs.

In Fig. 9 we show part of the data of Fig. 8 as function of the MHSP total effective gain (by varying $\mathrm{V_{ac}}$), for different $\mathrm{V_{hole}}$ values. The lowest ion back-flow ratio value increases very little with the total effective gain, from 17% to 25%, while the total gain increases by about three orders of magnitude, from $\sim$8 to 7×10^3.

The ion back-flow reduction due to the use of MHSP was demonstrated for a 3-GEMs/MHSP gaseous photomultiplier with a reflective CsI-photocathode evaporated on the top of the first GEM (Fig. 4). In this case all the back-flowing ions are collected at the photocathode, and the ion back-flow ratio was derived from the ratio between the photocathode ion current and the anode strips electron current. Fig. 10 depicts the ion back-flow ratio, as function of total effective gain (by varying $\mathrm{V_{ac}}$) of the photodetector.

Taking advantage of the very high multiplication of the MHSP, the ion back-flow in the 3-GEMs/MHSP cascade can be further reduced by reducing the transfer field above the MHSP, while maintaining sufficiently high total gain of the whole photodetector. As shown in Fig. 10, under such operating conditions, the ion back-flow ratio decreases to about 2% with total effective gains close to 10^6, sufficient for single-photon detection. This value compares favorably with the 20–30% ion back-flow ratio obtained in 4-GEMs photodetector at similar total effective gains [7].

D. 2-D Imaging

Reference [3] discusses the possibility of using the MHSP for 2-D imaging, where the anode strips provide one coordinate and the second coordinate is obtained by structuring the top electrode of the MHSP with orthogonal strips (see Fig. 2 of [3]). With suitable biasing voltages, the charge signal amplitude induced on the MHSP top electrode can have about 30%–50% of the anode-strip signal amplitude [8], [10], [11].

An alternative approach is to obtain the second coordinate, or both coordinates, from the positive ions collected at a patterned cathode plane placed a few hundred microns below the MHSP. Such approach is possible due to the large number of positive

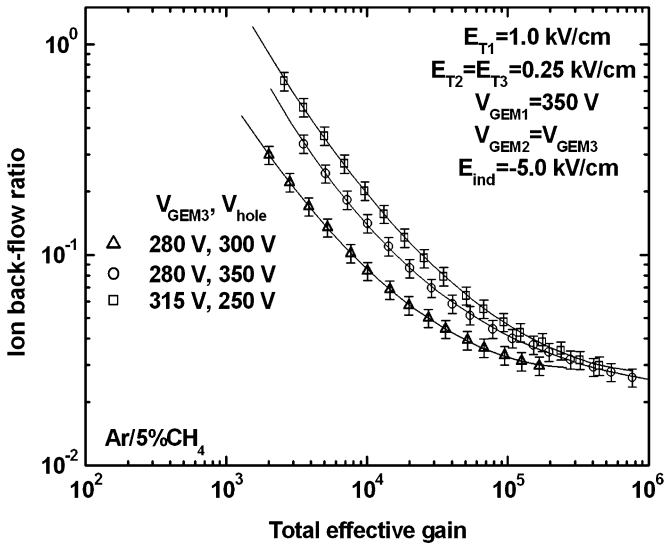

Fig. 10. Ratio between the number of ions collected on the reflective photocathode and the number of electrons collected at the anode strips, in a 3 GEMs/MHSP gaseous photomultiplier operated in $\mathrm{Ar}/5\%\mathrm{CH_4}$ gas mixture at 1 atm, as function of the total effective gain (by varying $\mathrm{V_{ac}}$), for several GEMs and $\mathrm{V_{hole}}$ voltages.

ions that can be diverted toward the cathode plane, of up to 50% of the number of electrons collected at the anode strips [6].

We explored this approach using a Wedge and Strip (W&S) readout cathode [12]–[14] of 1.6 mm pitch and an active area of $20 \times 20\ \mathrm{mm^2}$ [Fig. 11(b)]. It was placed at 0.4 mm behind a resistive electrode [15], [16], which in turn was placed at a distance of 0.5 mm from the MHSP. The resistive electrode (surface resistivity $\sim 1\ \mathrm{G\Omega/square}$) was made of 30 nm thick Ge-film deposited on a 1.5 mm thick G-10 frame [Fig. 11(a)]. Its role was to spread out the induced charge on the W&S readout electrode, and match the positive-ion cloud dimension (of $\sim$1 mm FWHM) to the W&S pitch, for correct position interpolation (i.e., induced-charge cloud diameter larger than the readout pitch). Unfortunately the resistive electrode was not optimized, and its signal transparency (measured by the ratio of the charge signal amplitudes with and without the resistive electrode, for the same electrostatic conditions in the detector) for the ions was only about 15%.

In Fig. 12 we present a photograph and the respective 2-D X-ray image of a stainless-steel slits-mask. It was placed above the radiation window of an X-ray detector (Fig. 11(a)), comprising a 2-GEMs/MHSP cascade in $\mathrm{Ar}/5\%\mathrm{CH_4}$ mixture at 1 atm. The image was obtained with 5.9-keV X-rays from a $^{55}\mathrm{Fe}$ source placed $\sim$70 cm above the mask, using the ions from the MHSP and reading their induced signals, with an apparent gain of 2×10^4, at the W&S readout behind the Ge-resistive layer. The apparent gain for signals recorded at the anode strips was $\sim 10^5$ (the difference being due to poor signal transparency of the resistive layer).

As seen in Fig. 12, slits that are 300 μm apart are well resolved. Position resolutions (FWHM) of the order of 200 and 250 μm were obtained for y- and x-coordinates, respectively. The limit from photoelectron and Auger electron range is $\sim$ 100 μm FWHM [17]. The present results are

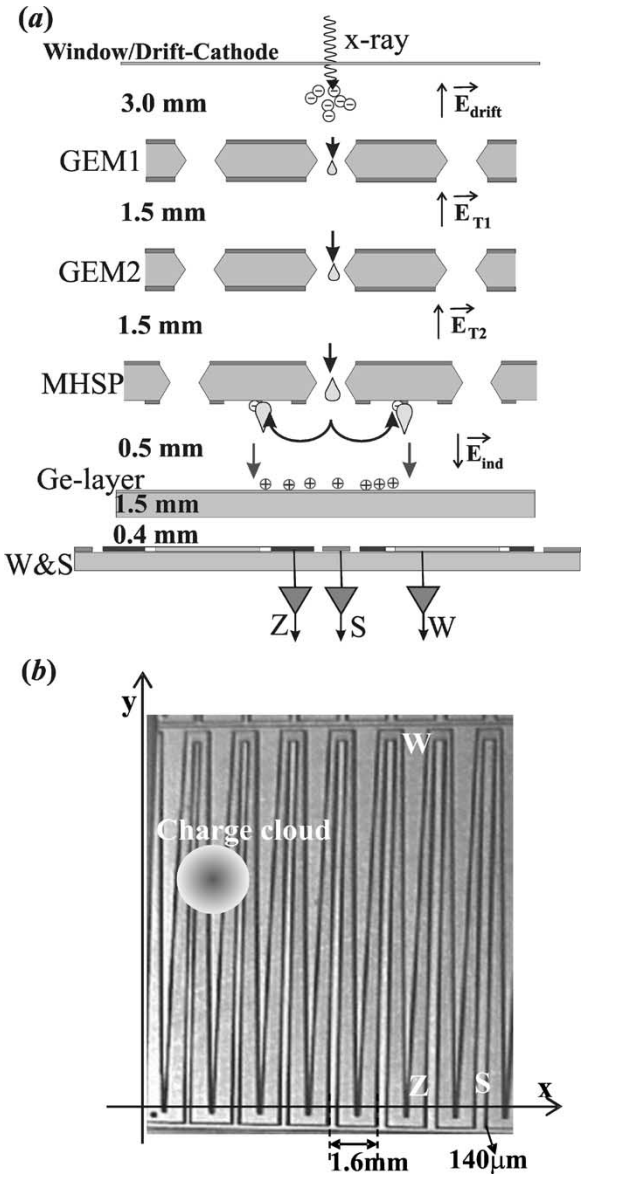

Fig. 11. Schematic view of the 2-GEMs/MHSP X-ray imaging detector (a), and a photomicrograph of the W&S electrode (b). The W&S structure has three independent electrodes; Z: Zigzag, W: Wedge and S: Strip. The charge cloud is shared by these electrodes and the x- and- y coordinates are determined from the fraction of charge collected on S and W, respectively.

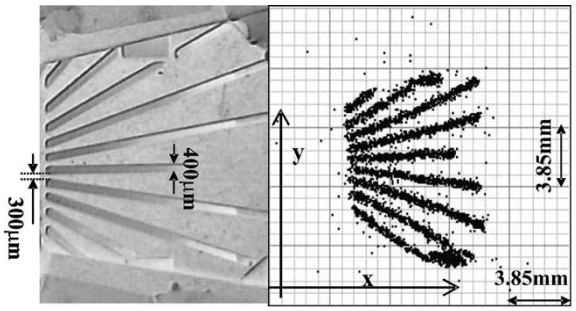

Fig. 12. Photograph (left) and respective 2-D X-ray image (right) of a stainless-steel slits-mask, placed above the radiation window of a gas detector instrumented with a 2-GEMs/MHSP cascade, in an $\mathrm{Ar}/5\%\mathrm{CH_4}$ mixture at 1 atm. The MHSP anode-strip width was 30 μm and the hole diameter was 40/60 μm in the Kapton/copper.

quite promising and may allow the use of this detector for single-photon imaging, as discussed in [11].

IV. Summary

The MHSP microstructure presents interesting characteristics in terms of gain, speed of response, photon-feedback suppression, and reduced ion back-flow. It can be used as a stand-alone multiplier for large radiation-induced charges or as a last element of a multi-GEM cascade; in the latter, gains as high as 10^7 were reached in $\mathrm{Ar}/5\%\mathrm{CH_4}$ gas mixture. Most important is the MHSP intrinsic capability to reduce ion back-flow, compared to that of the GEM. It originates from the fact that most ions from the anode-strip avalanche are collected at the nearby cathode strips and plane and only a small fraction of them, including those produced in the hole avalanche, backflow toward the MHSP upper region. Together with the high intrinsic gain of the MHSP, it permits reducing the ion back-flow in multi-GEM/MHSP multipliers down to 2% levels at gains close to 10^6. As $\sim$50% of the ions are directed toward the cathode plane below the MHSP, they could be useful for 2-D imaging with a structured cathode such as W&S electrode. Position resolutions (FWHM) of the order of 200 to 250 $\mu\mathrm{m}$ were demonstrated with soft X-rays.

A single MHSP-based detector presents good characteristics for X-ray detection. Its operation with Ar/5%Xe gas mixture have shown gains above 10^4 and energy resolutions of about 14% for 5.9-keV X-rays.

At present, the performance of MHSPs is limited (mainly the strip gain) by their manufacturing imperfections, which results also in low production-yield. It is expected, though, that MHSPs of better quality can be produced in the future and present superior performance to those obtained up to now.

Acknowledgment

The authors acknowledge V. Dangendorf for preparing the Ge resistive layer and for useful discussions. Two of the authors, J. M. Maia and J. F. C. A. Veloso, acknowledge support from FCT, Lisbon, Portugal. A. Breskin is the Reuther Professor of Research in peaceful use of atomic energy.

References

[1] F. Sauli, "GEM: a new concept for electron amplification in gas detectors," *Nucl. Instrum. Methods*, vol. A 386, pp. 531–534, 1997.

[2] A. Bressan, R. de Oliveira, A. Gandi, J. C. Labbe, L. Ropelewski, F. Sauli, D. Mörmann, T. Muller, and H. J. Simones, "Two-dimensional readout of GEM detectors," *Nucl. Instrum. Methods*, vol. A 425, pp. 254–261, 1999.

[3] J. F. C. A. Veloso, J. M. F. dos Santos, and C. A. N. Conde, "A proposed new microstructure for gas radiation detectors: the microhole and strip plate," *Rev. Sci. Instrum.*, vol. 71, pp. 2371–2376, 2000.

[4] J. M. Maia, J. F. C. A. Veloso, R. E. Morgado, J. M. F. dos Santos, and C. A. N. Conde, "The micro-hole- and -strip plate gas detector: experimental results," *IEEE Trans. Nucl. Sci.*, vol. 49, pp. 875–880, Apr. 2002.

[5] J. M. Maia, J. F. C. A. Veloso, J. M. F. dos Santos, A. Breskin, R. Chechik, and D. Mörmann, "Advances in the micro-hole & strip plate gaseous detector," *Nucl. Instrum. Methods*, vol. A 504, pp. 364–368, 2003.

[6] J. M. Maia, D. Mörmann, A. Breskin, R. Chechik, J. F. C. A. Veloso, and J. M. F. dos Santos, "Avalanche-ion back-flow reduction in gaseous electron multipliers based on GEM/MHSP," *Nucl. Instrum. Methods*, vol. A 523, pp. 334–344, 2004.

[7] D. Mörmann, A. Breskin, R. Chechik, and D. Bloch, "Evaluation and reduction of ion back-flow in multi-GEM detectors," *Nucl. Instrum. Methods*, vol. A 516, pp. 315–326, 2004.

[8] A. Oed, "Properties of micro-strip gas chambers (MSGC) and recent developments," *Nucl. Instrum. Methods*, vol. A 367, pp. 34–40, 1995.

[9] D. Mörmann, M. Balcerzyk, A. Breskin, R. Chechik, B. K. Singh, and A. Buzulutskov, "GEM-based gaseous photomultipliers for UV and visible photon imaging," *Nucl. Instrum. Methods*, vol. A 504, pp. 93–98, 2003.

[10] G. Cicognani, D. Feltin, B. Guerard, and A. Oed, "Study of the backside signal of micro-strip gas counters on electronic conducting glass," *IEEE Trans. Nucl. Sci.*, vol. 45, pp. 249–251, June 1998.

[11] J. M. Maia, D. Mörmann, A. Breskin, R. Chechik, J. F. C. A. Veloso, and J. M. F. dos Santos, "2D localization properties of GEM/MHSP radiation detectors," *Nucl. Instrum. Methods*, submitted for publication.

[12] O. H. W. Siegmund, S. Clothier, J. Thornton, J. Lemen, R. Harper, I. M. Mason, and J. L. Culhane, "Application of the wedge and strip anode to position sensing with microchannel plates and proportional counters," *IEEE Trans. Nucl. Sci.*, vol. NS-30, pp. 503–507, 1983.

[13] O. H. W. Siegmund, M. Lampton, J. Bixler, S. Bowyer, and R. F. Malina, "Operational characteristics of wedge and strip image readout systems," *IEEE Trans. Nucl. Sci.*, vol. NS-33, pp. 724–727, 1986.

[14] C. Martin, P. Jelinsky, M. Lampton, R. F. Malina, and H. O. Anger, "Wedge-and-strip anodes for centroid-finding position-sensitive photon and particle detectors," *Rev. Sci. Instrum.*, vol. 52, pp. 1067–1074, 1981.

[15] G. Battistoni, P. Campana, V. Chiarella, U. Denni, E. Iarocci, and G. Nicoletti, "Resistive cathode transparence," *Nucl. Instrum. Methods*, vol. 202, pp. 459–464, 1982.

[16] V. Dangendorf, private communication, 2003.

[17] J. Fischer, V. Radeka, and G. C. Smith, "X-ray position detection in the region of 6 $\mu\mathrm{m}$ RMS with wire proportional chambers," *Nucl. Instrum. Methods*, vol. A 252, pp. 239–245, 1986.